blood

RED CELLS, IRON, AND ERYTHROPOIESIS

Endothelial cells produce bone morphogenetic protein 6 required for iron homeostasis in mice

Susanna Canali,[1,2] Kimberly B. Zumbrennen-Bullough,[1,2] Amanda B. Core,[1,2] Chia-Yu Wang,[1,2] Manfred Nairz,[2] Richard Bouley,[1,2] Filip K. Swirski,[2] and Jodie L. Babitt[1,2]

[1]Program in Anemia Signaling Research, Division of Nephrology, Program in Membrane Biology, and [2]Center for Systems Biology, Massachusetts General Hospital, Harvard Medical School, Boston, MA

Key Points

- Endothelial *Bmp6* conditional knockout mice exhibit hemochromatosis, whereas hepatocyte and macrophage *Bmp6* conditional knockout mice do not.

- Our data support a model in which EC Bmp6 has paracrine actions on hepatocyte hemojuvelin to regulate hepcidin production.

Bone morphogenetic protein 6 (BMP6) signaling in hepatocytes is a central transcriptional regulator of the iron hormone hepcidin that controls systemic iron balance. How iron levels are sensed to regulate hepcidin production is not known, but local induction of liver BMP6 expression by iron is proposed to have a critical role. To identify the cellular source of BMP6 responsible for hepcidin and iron homeostasis regulation, we generated mice with tissue-specific ablation of *Bmp6* in different liver cell populations and evaluated their iron phenotype. Efficiency and specificity of Cre-mediated recombination was assessed by using Cre-reporter mice, polymerase chain reaction of genomic DNA, and quantitation of *Bmp6* messenger RNA expression from isolated liver cell populations. Localization of the BMP co-receptor hemojuvelin was visualized by immunofluorescence microscopy. Analysis of the *Bmp6* conditional knockout mice revealed that liver endothelial cells (ECs) expressed *Bmp6*, whereas resident liver macrophages (Kupffer cells) and hepatocytes did not. Loss of *Bmp6* in ECs recapitulated the hemochromatosis phenotype of global *Bmp6* knockout mice, whereas hepatocyte and macrophage *Bmp6* conditional knockout mice exhibited no iron phenotype. Hemojuvelin was localized on the hepatocyte sinusoidal membrane immediately adjacent to Bmp6-producing sinusoidal ECs. Together, these data demonstrate that ECs are the predominant source of BMP6 in the liver and support a model in which EC BMP6 has paracrine actions on hepatocyte hemojuvelin to regulate hepcidin transcription and maintain systemic iron homeostasis. (*Blood*. 2017;129(4):405-414)

Introduction

Iron homeostasis is tightly controlled to ensure sufficient iron for erythropoiesis and other fundamental metabolic processes and to prevent the toxicity of excess iron.[1] The peptide hormone hepcidin is a master regulator of systemic iron balance by mediating the degradation of the iron export protein ferroportin to limit dietary iron absorption and macrophage iron recycling.[2] Hepcidin production in the liver is carefully titrated in response to changes in organismal iron content and iron utilization requirements.[1] Failure to appropriately induce hepcidin in response to iron is a central feature of hereditary hemochromatosis, a genetic disorder characterized by excess iron deposits in the liver, heart, and endocrine glands, resulting in organ dysfunction.[3] The most severe juvenile-onset form of this disease is caused by mutations in the genes encoding hepcidin itself (*HAMP*) or hemojuvelin (*HFE2*, also known as *HJV*), which regulates hepcidin transcription in hepatocytes.[4,5] Mice with global or hepatocyte-specific deletion of these genes have a similar iron overload phenotype,[6-11] confirming the essential role of hepatocyte hepcidin production regulated by HJV in controlling systemic iron balance.

HJV regulates hepcidin by functioning as a co-receptor for the BMP signaling pathway,[12] which activates hepcidin transcription via specific SMAD-binding elements on the hepcidin promoter.[13] BMP6 is a key endogenous ligand for HJV to regulate hepcidin transcription and systemic iron balance because global $Bmp6^{-/-}$ mice exhibit an iron overload phenotype similar to that of $Hjv^{-/-}$ mice.[14,15] Moreover, heterozygous mutations in the *BMP6* prodomain were recently linked to inappropriately low hepcidin levels and iron overload in humans.[16] Notably, liver *Bmp6* messenger RNA (mRNA) expression is regulated by dietary iron and correlates with liver iron content in mice, whereas *Bmp6* expression is not altered by iron in other tissues.[17-21] In addition, a neutralizing BMP6 antibody blunts hepcidin induction by a high iron diet, resulting in increased accumulation of tissue iron in mice.[18] Thus, regulation of liver *BMP6* mRNA expression is a critical mechanism by which iron levels regulate hepcidin.

How iron levels are sensed by the liver to control BMP6 production remains unknown. Liver cell isolation experiments suggest that nonparenchymal cells (NPCs), including sinusoidal endothelial cells (SECs), Kupffer cells (KCs), and hepatic stellate cells (HSCs) rather than hepatocytes, are the predominant source of BMP6 in the liver.[22-24] However, *Bmp6* mRNA and protein were reported to be induced by

---

iron in hepatocytes.[19,24,25] Importantly, functional data are lacking that demonstrate which liver cell population is the main source of BMP6 that is crucial for maintaining systemic iron balance. To answer this fundamental question, we generated mice with a conditional knockout of *Bmp6* in different liver cell populations.

Methods

Animals

Animal protocols were approved by the Institutional Animal Care and Use Committee at Massachusetts General Hospital. Embryonic stem (ES) cells from 129SvEv mice expressing a *Bmp6* floxed allele (Figure 1A) were purchased from Mutant Mouse Resource and Research Center (Lexicon 1E10, 029763-UCD). ES cells were injected into C57BL/6 blastocysts to generate chimeric mice by the Beth Israel Deaconess Transgenic Core Facility. Chimeric mice were mated with C57BL/6 mice to generate F1 heterozygotes, which were intercrossed to generate littermate *Bmp6*^{+/+} (wild-type), *Bmp6*^{fl/+}, and *Bmp6*^{fl/fl} (*Bmp6* floxed) mice.

To generate global *Bmp6* knockout (*Bmp6*^{−/−}) mice, *Bmp6*^{fl/fl} mice were mated with mice expressing Cre recombinase under a global cytomegalovirus (CMV) promoter (B6.C-Tg(CMV-cre)1Cgn/J; The Jackson Laboratory). *Bmp6*^{+/−};CMV-Cre+ offspring were crossed with C57BL/6 mice to ensure germline transmission and remove the Cre. *Bmp6*^{+/−} offspring were intercrossed to generate littermate *Bmp6*^{+/+}, *Bmp6*^{+/−}, and *Bmp6*^{−/−} mice.

To generate conditional *Bmp6* knockout (*Bmp6*^{fl/fl};Cre+) mice, *Bmp6*^{fl/fl} mice were crossed with mice (The Jackson Laboratory) expressing Cre recombinase under the control of an albumin promoter/enhancer (B6.Cg-Tg (Alb-cre)21Mgn/J, hereafter Alb-Cre), receptor tyrosine kinase Tek (Tie2) promoter/enhancer (B6.Cg-Tg(Tek-cre)1Ywa/J, hereafter Tek-Cre), or lysozyme 2 gene (Lyz2) promoter/enhancer elements (B6.129P2-Lyz2[tm1(cre)Ifo]/J, hereafter LysM-Cre). Efficiency and specificity of Cre-mediated recombination was assessed by mating Alb-Cre, Tek-Cre, and LysM-Cre mice with Cre-reporter mice (B6.Cg-Gt(ROSA)26Sor[tm9(CAG-tdTomato)Hze]/Jackson, hereafter *Rosa26*[tdT]) that express tandem dTomato (tdT) in Cre+ cells because of removal of a *LoxP*-flanked stop cassette.

All mice were maintained on a mixed C57BL/6,129SvEv background with ad libitum access to water and a Prolab 5P75 Isopro RMH 3000 diet containing 380 ppm iron. Mice were genotyped by polymerase chain reaction (PCR) of genomic DNA extracted from the tail and from isolated liver cell populations using a DNeasy Blood Tissue Kit (Qiagen) and primers listed in supplemental Table 1, available on the *Blood* Web site. Age- and sex-matched littermate *Bmp6*^{+/+} or *Bmp6*^{fl/fl};Cre− mice were used as controls throughout the study. Numbers, sex, and ages of mice used in experiments are listed in supplemental Table 2.

Immunofluorescence microscopy

Liver sections were fixed, cryosectioned, and stained with anti-CD31, anti-F4/80, anti-desmin, and anti-HJV antibodies as detailed in the supplemental Methods. Images were acquired by using a Nikon A1R confocal laser scanning microscope. TIFF files were imported into Adobe Photoshop, and the entire field was enhanced and sharpened by using the levels command and/or high-pass filter. Recombination efficiency was quantitated by counting the percent of hepatocytes, KCs, and SECs (determined by morphology, F4/80, or CD31 staining, respectively) that were tdT positive in *Rosa26*[tdT];Alb-Cre-, LysM-Cre-, and Tek-Cre-reporter mice. In all, 325 to 1000 cells were counted in 4 mice per group.

Hepatocyte and NPC isolation

Livers were perfused via the inferior vena cava with KRH (115 mM NaCl, 5 mM KCl, 1 mM KH2PO4, 25 mM N-2-hydroxyethylpiperazine-N′-2-ethanesulfonic acid [pH 7.4]) containing 0.02% EGTA at 5 mL/min for 7 minutes, followed by 0.005% collagenase (Sigma-Aldrich), 1 mM CaCl2, and 2.5 mM MgSO4 in KRH for 6 minutes. Cells were filtered through a 70-μm cell strainer and centrifuged at 50 rcf for 4 minutes. The supernatant was centrifuged at 750 rcf for 5 minutes to
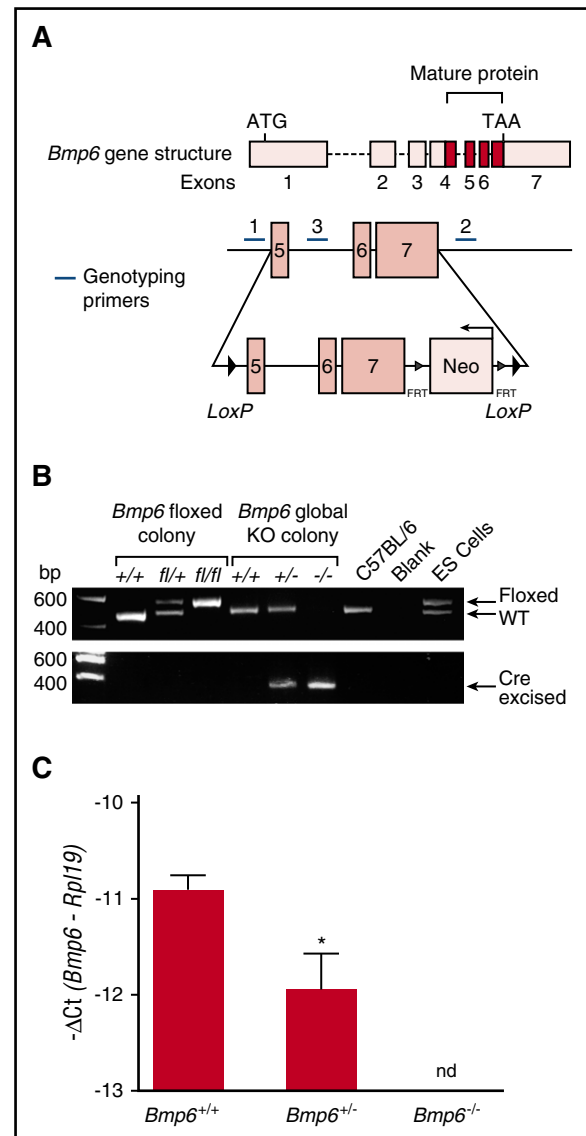
Figure 1. Generation of *Bmp6* floxed (*Bmp6*^{fl/fl}) and *Bmp6*^{−/−} global knockout mice. (A) Schematic representation of *Bmp6* gene structure and the floxed *Bmp6* allele. Cre-mediated excision of exons 5 to 7 encoding the mature Bmp6 protein generates a functionally null allele. Genotyping primer positions are indicated. (B) PCR of tail genomic DNA from *Bmp6* floxed and global knockout mouse colonies shows the presence of wild-type (WT) (+), floxed (fl), and cre-excised (−) alleles. (C) qRT-PCR of liver *Bmp6* relative to *Rpl19* mRNA in the *Bmp6*^{+/+}, *Bmp6*^{+/−}, and *Bmp6*^{−/−} mice (n = 7 to 11 males and 5 to 7 females per group; supplemental Table 2). Results are reported as mean ± standard error of the mean (SEM) of −ΔCt = −[Ct target mRNA − Ct *Rpl19*], with a higher −ΔCt indicating higher mRNA expression. Fold change in mRNA expression between groups is calculated by 2^(−ΔΔCt), where ΔΔCt = ΔCt higher expressing group − ΔCt lower expressing group. *P < .05 relative to *Bmp6*^{+/+} mice by Student t test. nd, not detectable.

collect NPCs, and pellets were resuspended in KRH and centrifuged in a 50% Percoll gradient (GE Healthcare) at 50 rcf for 10 minutes to collect viable hepatocytes.

KC and endothelial cell isolation

NPC supernatants collected as above were filtered through a 40-μm cell strainer, centrifuged at 750 rcf for 5 minutes, and treated with red blood cell lysis buffer (BioLegend). Cell pellets were resuspended and stained in phosphate-buffered saline containing 1% fetal bovine serum and 0.5% bovine serum albumin using antibodies listed in supplemental Table 3. KCs and endothelial cells (ECs; composed mainly of SECs) were isolated by fluorescence-activated cell sorting (FACS) using a FACSAria II (BD Biosciences). Cells were first gated using

forward scatter and side scatter characteristics, and doublets were sequentially excluded by comparing foward scatter and side scatter height and area signals. ECs were identified as CD326⁻, CD45⁻, CD31⁺, CD146⁺. KCs were defined as CD326⁻, CD31⁻, CD45⁺, Lin⁻, F4/80^high, CD11b^int, CD64⁺, MHC-II⁺, after separation from lineage-positive leukocytes (CD3e, CD19, CD90.2, Ly6G, NK1.1) and monocytes (CD326⁻, CD31⁻, CD45⁺, Lin⁻, F4/80^low, CD11b⁺, CD64⁻ Ly-6C⁺). For purity checks, sorted cell populations were run on an LSRII flow cytometer (BD Biosciences), and data were analyzed with FlowJo v8.8.6 software (Tree Star).

RNA isolation and quantitative real-time reverse transcription PCR

Total liver RNA was isolated by using QIAshredder and RNeasy purification kits (Qiagen), and complementary DNA (cDNA) was synthesized from 1000 ng RNA by using the iScript cDNA synthesis kit (Bio-Rad). For isolated liver cell populations, RNA was extracted with the PicoPure RNA Isolation Kit (Thermo Scientific), RNA concentration was measured with an RNA 6000 Pico Kit and 2100 Bioanalyzer (Agilent), and cDNA was synthesized from 1000 pg RNA by using the SuperScript VILO cDNA Synthesis Kit (Invitrogen) according to the manufacturers' instructions. Quantitative real-time PCR was performed as described previously[26] by using the Power SYBR Green PCR Master Mix (Life Technologies) and primers listed in supplemental Table 4. Results are reported as mean ± standard error of the mean using the formula $-\Delta Ct = -[Ct\ target\ gene - Ct\ control\ gene\ Rpl19]$, with a higher $-\Delta Ct$ indicating higher mRNA expression. Fold change is derived from $2^{-\Delta\Delta Ct}$ where $\Delta\Delta Ct = \Delta Ct$ higher expressing group $- \Delta Ct$ lower expressing group.

Iron analysis

Serum iron, transferrin saturation, and tissue nonheme iron concentrations were determined as described previously.[26] Tissue iron is reported as micrograms of iron per gram of wet weight tissue.

Prussian blue staining

Tissues were fixed in neutral buffered formalin for 24 hours, embedded in paraffin, sectioned at 7 μm, deparaffinized and rehydrated, and subjected to Perls' Prussian blue staining by using an iron stain kit (American MasterTech). For tissues with less iron loading, a modified diaminobenzidine-enhanced Perls' stain containing cobalt chloride was used.[27]

Statistics

Statistical significance was determined by two-tailed Student t test or one-way analysis of variance (ANOVA) with Dunnett's or Tukey's post hoc test for pairwise multiple comparisons using Prism 7 (GraphPad). $P < .05$ was considered significant.

Results

Generation of Bmp6^fl/fl, Bmp6^−/−, and conditional Bmp6 knockout mice

Bmp6 chimeric mice were generated by injecting C57BL/6 blastocysts with 129SvEv ES cells containing a recombined Bmp6 allele with LoxP sites flanking exons 5 to 7 encoding the Bmp6 mature region (Figure 1A). Germline transmission was confirmed by PCR (Figure 1B). Bmp6^fl/+ mice were intercrossed to generate littermate Bmp6^fl/fl and Bmp6^+/+ mice on a mixed C57BL/6,129SvEv background. Bmp6^fl/fl mice exhibited iron parameters similar to that of littermate Bmp6^+/+ mice without other obvious abnormalities, suggesting that the floxed allele does not impact Bmp6 function (supplemental Figure 1).

Bmp6^fl/fl mice were mated with C57BL/6 mice expressing Cre recombinase under a global CMV promoter (see "Methods") to generate littermate Bmp6^+/+, Bmp6^+/−, and Bmp6^−/− mice on a mixed C57BL/6,129SvEv background. Genotyping showed the expected wild-type and recombined alleles (Figure 1B). qRT-PCR of liver tissue confirmed a progressive loss of Bmp6 mRNA expression in Bmp^+/− and Bmp6^−/− mice (Figure 1C).

To generate mice lacking Bmp6 in different liver cell populations, Bmp6^fl/fl mice were mated with Alb-Cre, LysM-Cre, or Tek-Cre mice (see "Methods"), which have been widely used in the literature to generate hepatocyte, macrophage, and endothelial conditional knock-out mice, respectively.[28-30] HSC conditional knockout mice were not generated because of the lack of commercially available HSC-specific Cre mice. All Bmp6 conditional knockout mice (Bmp6^fl/fl;Cre+) were compared with littermate Bmp6^fl/fl;Cre− mice.

Efficiency and specificity of Cre-mediated recombination were evaluated by immunofluorescence microscopy of liver tissue from tdT Cre-reporter mice (Rosa26^tdT) mated with each Cre strain by using antibodies against CD31, desmin, and F4/80 to identify SECs, HSCs, and KCs, respectively (Figure 2A-C). Hepatocytes were identified by cell morphology. tdT was expressed specifically in hepatocytes in Alb-Cre mice (Figure 2A) and in macrophages in LysM-Cre mice (Figure 2B), with recombination efficiencies of >99% and 98%, respectively, consistent with previous studies.[31,32] In offspring from a male Tek-Cre parent, tdT was highly expressed in SECs (Figure 2C) with 98% recombination efficiency, but low-level expression was also seen in KCs (Figure 2C, inset). This is consistent with a recent report that KCs originate from Tek-expressing progenitors in the yolk sac.[33] Notably, some offspring from female Tek-Cre mice exhibited germline recombination as previously reported.[34] Therefore, we used only offspring from a male Tek-Cre parent for subsequent analyses.

Bmp6 recombination was evaluated by PCR of genomic DNA from isolated liver cell populations. ECs and KCs were each isolated by FACS and exhibited ≥99% purity as measured by FACS (supplemental Figure 2). qRT-PCR of Cd146, Cd45, and Tmprss6 as markers of ECs, leukocytes including KCs, and hepatocytes, respectively, confirmed that the isolated cell populations were highly enriched with ~40- to 400-fold higher levels of the cell type–specific transcripts in the corresponding cell populations (Figure 2D-F). However, Cd146, Cd45, and Tmprss6 were still detectable in non-EC, non-KC, and nonhepatocyte fractions, respectively, suggesting some contamination of each cell population with RNA from all of the other cell types. Despite these minor impurities, PCR of genomic DNA confirmed the loss of the floxed allele and the presence of the recombined allele specifically in hepatocytes for Bmp6^fl/fl;Alb-Cre+ mice (Figure 2G) and KCs for Bmp6^fl/fl;LysM-Cre+ mice (Figure 2H). Bmp6^fl/fl;Tek-Cre+ mice exhibited loss of the floxed allele and presence of the recombined allele in both ECs and KCs (Figure 2I).

Loss of Bmp6 mRNA expression in isolated liver cell populations was assessed by qRT-PCR. In control Bmp6^fl/fl;Cre− mice, Bmp6 mRNA was much more abundant in NPCs than in hepatocytes and was predominantly expressed in ECs. (Figure 2J-L). Notably, the fold enrichment of Bmp6 mRNA in ECs relative to hepatocytes and KCs was similar to the fold enrichment of the endothelial marker Cd146 (compare Figure 2J-L Bmp6^fl/fl;Cre− mice to 2D). This suggests that the Bmp6 measured in hepatocyte and KC fractions could be the result of EC contamination. Consistent with the Cre-reporter mice and genomic DNA results, Bmp6 mRNA was strongly reduced in ECs and KCs of Bmp6^fl/fl;Tek-Cre+ mice (Figure 2L). Interestingly, the relatively low Bmp6 mRNA expression was not further reduced in hepatocytes of Bmp6^fl/fl;Alb-Cre+ mice (Figure 2J) or in KCs of Bmp6^fl/fl;LysM-Cre+ mice (Figure 2K), despite clear Cre-mediated
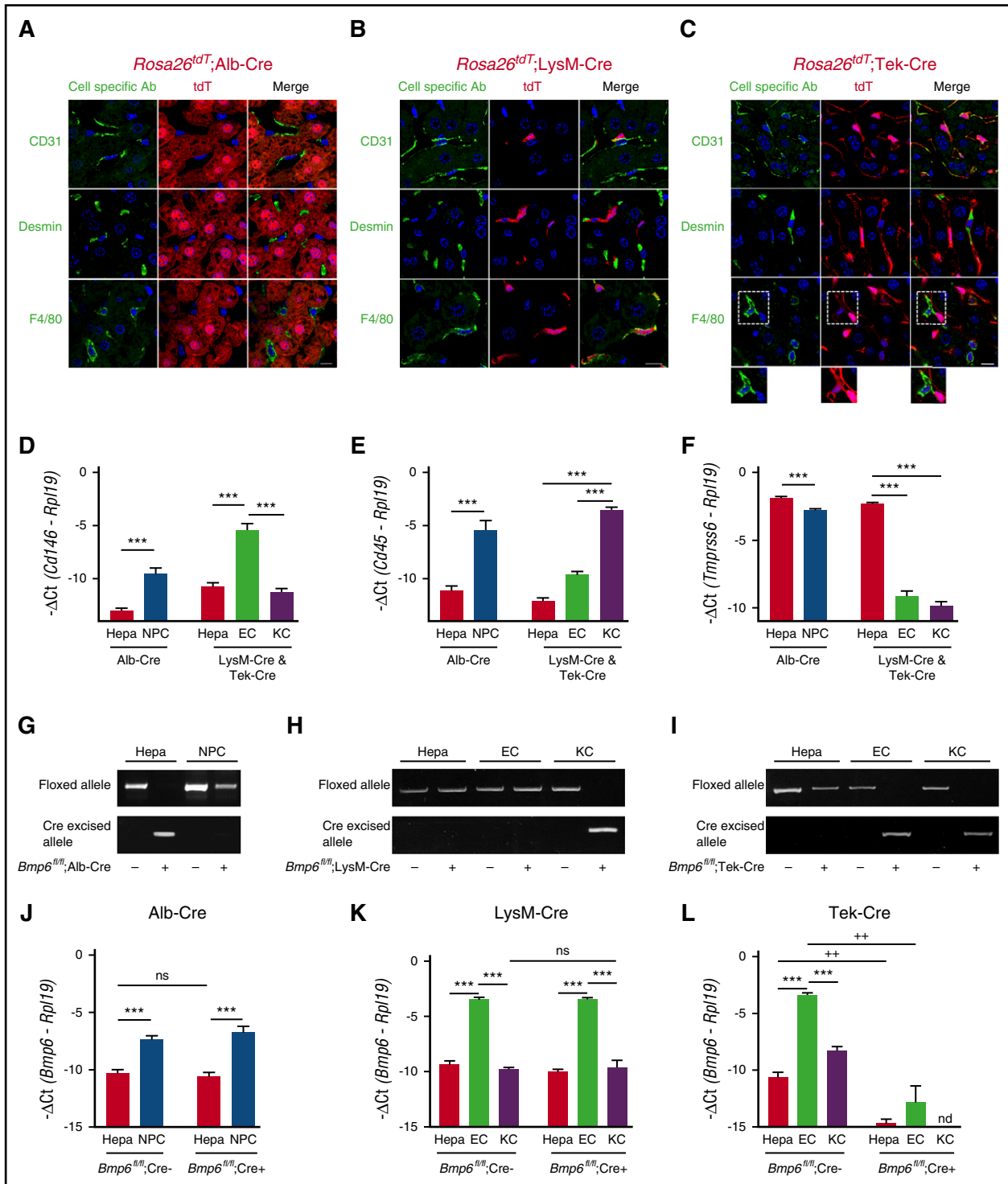
Figure 2. Validation of conditional *Bmp6* knockout mice. (A-C) Immunofluorescence microscopy of liver from offspring of *Rosa26*^{tdT} Cre-reporter mice mated with (A) Alb-Cre, (B) LysM-Cre, and (C) Tek-Cre mice. Cells expressing Cre recombinase are labeled red throughout the cytoplasm because of the removal of a stop codon upstream of the tdT fluorescent protein. Other NPC populations are labeled green by using CD31 (ECs), desmin (HSCs), and F4/80 (KCs) antibodies. Nuclei are labeled blue with 4′,6-diamidino-2-phenylindole (DAPI). Dotted areas are shown with increased brightness below the right panel. Scale bars represent 10 μM. One representative mouse of 4 to 7 per group is shown. (D-F,J-L) qRT-PCR of (D) the EC marker *Cd146*, (E) the leukocyte/KC marker *Cd45*, (F) the hepatocyte (Hepa) marker *Tmprss6*, and (J-L) *Bmp6* relative to *Rpl19* mRNA from isolated hepatocytes, NPCs, ECs, or KCs from *Bmp6* conditional knockout and littermate control *Bmp6*^{fl/fl};Cre– mice (n = 3-5 per group). Results are reported as mean ± SEM of –ΔCt as in Figure 1. (G-I) PCR of genomic DNA for floxed and cre-excised *Bmp6* alleles from isolated hepatocytes, NPCs, ECs, or KCs from *Bmp6* conditional knockout and littermate control *Bmp6*^{fl/fl};Cre– mice (n = 3-5 per group). Representative gels are shown. ***$P < .001$ for NPCs relative to hepatocytes by Student *t* test or for ECs relative to hepatocytes or KCs by one-way ANOVA with Tukey post hoc test for mice of the same genotype. ++$P < .01$ in *Bmp6*^{fl/fl};Cre+ relative to *Bmp6*^{fl/fl};Cre– mice for the same cell type by Student *t* test. nd, not detectable; ns, not significant.
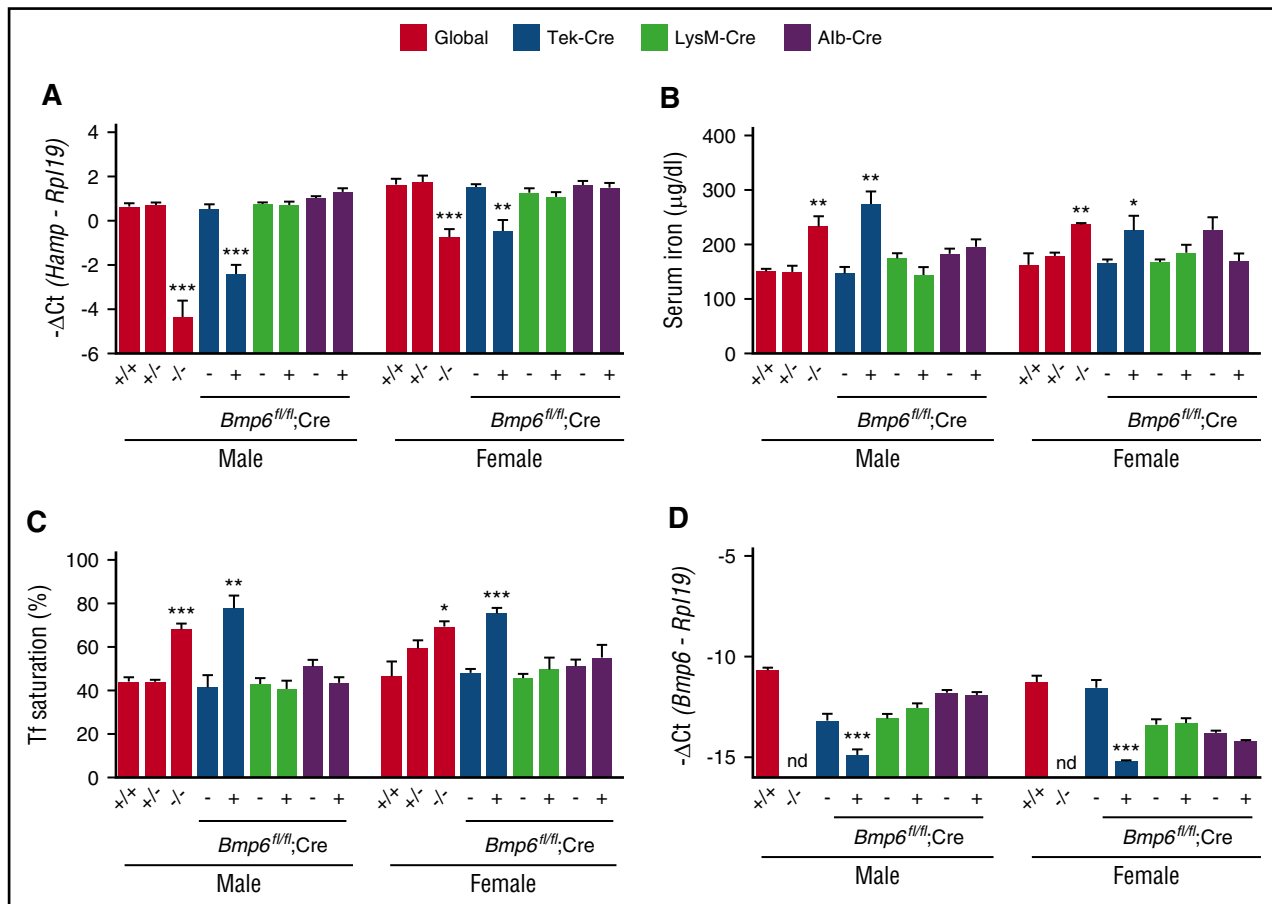
Figure 3. Eight-week-old *Bmp6*^{fl/fl};Tek-Cre+ mice exhibit liver *Bmp6* and *Hamp* deficiency and serum iron overload, whereas *Bmp6*^{fl/fl};Alb-Cre+ and *Bmp6*^{fl/fl}; LysM-Cre+ mice do not. Eight-week-old littermate male (left) and female (right) *Bmp6*$^{+/+}$, *Bmp6*$^{+/-}$, and *Bmp6*$^{-/-}$ global knockout mice (red bars) and *Bmp6* conditional knockout mice in ECs (*Bmp6*$^{fl/fl}$;Tek-Cre+ [blue bars]), macrophages (*Bmp6*$^{fl/fl}$;LysM-Cre+ [green bars]), and hepatocytes (*Bmp6*$^{fl/fl}$;Alb-Cre+ [purple bars]) compared with littermate controls (*Bmp6*$^{fl/fl}$;Cre–) were analyzed for (A) total liver hepcidin (*Hamp*) and (D) *Bmp6* relative to *Rpl19* mRNA by qRT-PCR, (B) serum iron, and (C) transferrin (Tf) saturation. n = 4-11 mice per sex per group (supplemental Table 2). Results are reported as mean ± SEM of −ΔCt as in Figure 1. *Bmp6* mRNA levels for *Bmp6*$^{+/+}$ and *Bmp6*$^{-/-}$ mice, stratified by sex, were replotted from Figure 1 for comparison. *$P <$ .05, **$P <$ .01, ***$P <$ .001 relative to control *Bmp6*$^{+/+}$ mice or *Bmp6*$^{fl/fl}$;Cre– mice by one-way ANOVA with Dunnett's post hoc test or Student *t* test. nd, not detectable.

recombination in the Cre-reporter mice and genomic DNA analysis (Figure 2A-B,G-H). In contrast, *Bmp6* mRNA expression was almost completely abolished in hepatocytes of *Bmp6*^{fl/fl};Tek-Cre+ mice (Figure 2L), despite the absence of Cre-mediated recombination in hepatocytes by Cre-reporter mice and genomic DNA analysis (Figure 2C,I). Together, these data suggest that ECs are the predominant source of BMP6 in the liver, whereas the hepatocyte and KC *Bmp6* mRNA measured here and reported in other cell isolation studies[22-24] is most likely an artifact of EC contamination. Importantly, although the Tek-Cre causes recombination in KCs as well as ECs (this appears to be a limitation of all endothelial models described to date), the recombination of *Bmp6* in KCs is unlikely to be of functional significance.

Bmp6^{fl/fl};Tek-Cre+ mice exhibit hepcidin deficiency and iron overload, whereas *Bmp6*^{fl/fl};Alb-Cre+ and *Bmp6*^{fl/fl};LysM-Cre+ mice do not

A hemochromatosis phenotype was previously reported for *Bmp6*$^{-/-}$ mice generated by a different strategy that targeted exon 2.[14,15] *Bmp6*$^{-/-}$ mice in this study likewise exhibited significantly reduced liver hepcidin (*Hamp*) mRNA (Figure 3A [red bars]), increased serum iron and transferrin saturation (Figure 3B-C [red bars]), increased liver iron (Figure 4A [compare red with magenta lines] and C; supplemental

Figure 3), reduced spleen iron (Figure 4B [compare red with magenta lines] and C; supplemental Figure 3), and increased extrahepatic iron loading in pancreas and heart (Figure 5; supplemental Figure 3) compared with littermate *Bmp6*$^{+/+}$ mice at 8 to 16 weeks of age. The *Bmp6* target transcript *Id1*, but not *Smad7*, was also reduced in *Bmp6*$^{-/-}$ mice (supplemental Figure 4). Both male and female *Bmp6*$^{-/-}$ mice exhibited hemochromatosis; however, male *Bmp6*$^{-/-}$ mice seemed to have lower *Hamp* mRNA (Figure 3A) and greater extrahepatic iron loading compared with female *Bmp6*$^{-/-}$ mice (Figure 5), similar to a prior report.[35] Heterozygous *Bmp6*$^{+/-}$ mice did not have an iron overload phenotype.

Bmp6$^{fl/fl}$;Tek-Cre+ mice also exhibited significantly lower liver *Bmp6* and *Hamp* mRNA, increased serum iron and transferrin saturation, increased liver iron, reduced spleen iron, and increased extrahepatic iron loading compared with littermate *Bmp6*$^{fl/fl}$;Cre– mice (Figures 3 [blue bars], 4A-B, and 5A-B [compare dark blue to light blue lines], 4C, 5C; supplemental Figure 3). Similar to *Bmp6*$^{-/-}$ mice, males seemed to have greater *Hamp* mRNA deficiency (Figure 3A) and extrahepatic iron loading (Figure 5) compared with females. Although a comparative analysis of *Bmp6*$^{-/-}$ and *Bmp6*$^{fl/fl}$;Tek-Cre+ mice is limited by their mixed genetic background and the inability to compare littermates, *Bmp6*$^{fl/fl}$;Tek-Cre+ mice had detectable residual liver *Bmp6* mRNA, whereas *Bmp6*$^{-/-}$ mice did not (Figure 3D). Consistent with some residual
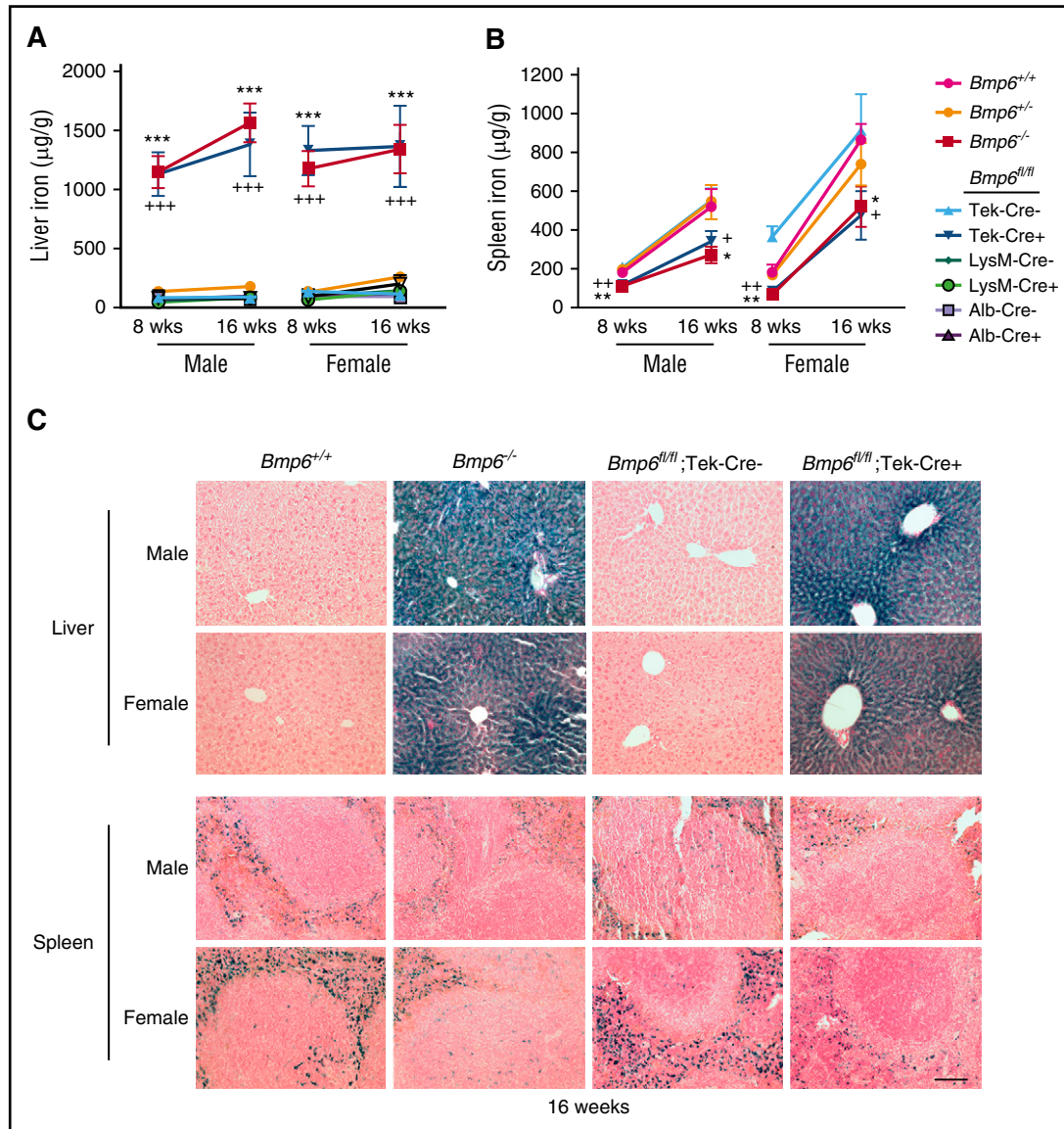
Figure 4. Liver iron is increased and spleen iron is reduced in *Bmp6*^{fl/fl};Tek-Cre+ mice, but not *Bmp6*^{fl/fl};Alb-Cre+ or *Bmp6*^{fl/fl};LysM-Cre+ mice. Eight- and 16-week-old littermate male and female *Bmp6*^{+/+}, *Bmp6*^{+/−}, and *Bmp6*^{−/−} global knockout mice and *Bmp6* conditional knockout mice in ECs (*Bmp6*^{fl/fl};Tek-Cre+), macrophages (*Bmp6*^{fl/fl};LysM-Cre+), and hepatocytes (*Bmp6*^{fl/fl};Alb-Cre+) compared with littermate controls (*Bmp6*^{fl/fl};Cre–) were analyzed for tissue iron in (A,C) liver and (B,C) spleen by (A-B) biochemical analysis or (C) Perls' Prussian blue. n = 4-7 mice per group (supplemental Table 2), with tissues from 1 representative mouse shown in (C) (original magnification ×20; scale bar represents 100 μM). *$P < .05$, **$P < .01$, ***$P < .001$ relative to control *Bmp6*^{+/+} mice by one-way ANOVA with Dunnett's post hoc test; +$P < .05$, ++$P < .01$, +++$P < .001$ relative to control *Bmp6*^{fl/fl};Cre– mice by Student t test.

Bmp6 activity, *Bmp6*^{fl/fl};Tek-Cre+ mice tended to have higher *Hamp* mRNA, particularly in males, and lower extrahepatic iron loading compared with sex-matched *Bmp6*^{−/−} mice (Figures 3A and 5).

In contrast, *Bmp6*^{fl/fl};LysM-Cre+ and *Bmp6*^{fl/fl};Alb-Cre+ mice had normal serum and tissue iron levels and unchanged liver *Hamp* and *Bmp6* mRNA expression compared with littermate *Bmp6*^{fl/fl};Cre– mice, even up to 16 weeks of age (Figures 3 [green and purple bars], 4, and 5; supplemental Figure 5). Moreover, no differences were seen in *Hamp* mRNA induction or serum or tissue iron levels in *Bmp6*^{fl/fl};Alb-Cre+ or *Bmp6*^{fl/fl};LysM-Cre+ mice compared with *Bmp6*^{fl/fl};Cre– mice in response to a high iron diet (supplemental Figure 6). Although the high iron diet seemed to increase *Bmp6* mRNA in all isolated liver cell populations, as previously reported,[24] *Bmp6* mRNA was still not reduced in isolated hepatocytes of *Bmp6*^{fl/fl};Alb-Cre+ or in the KCs of *Bmp6*^{fl/fl};LysM-Cre+ mice compared with *Bmp6*^{fl/fl};Cre– mice, whereas

Bmp6 mRNA was reduced in all cell populations from *Bmp6*^{fl/fl};Tek-Cre+ mice (supplemental Figure 7). The relative *Bmp6* mRNA expression in different liver cell populations of *Bmp6*^{fl/fl};Cre– mice continued to mirror the relative expression of the EC marker *Cd146* (supplemental Figure 7). These data are consistent with the notion that measured *Bmp6* mRNA in isolated hepatocytes and KCs is an artifact of EC contamination and suggest that hepatocytes and KCs do not functionally contribute to liver Bmp6 production, even in the context of iron loading. As previously reported,[18-21] the induction of *Bmp6* mRNA by using a high iron diet appeared to be limited to the liver because we did not detect increases in *Bmp6* mRNA in other organs tested, including the heart (supplemental Figure 8).

Paracrine effects of SEC Bmp6 on hepatocyte Hjv

Finally, we examined localization of the Bmp6 co-receptor Hjv in the livers of mice expressing the tdT reporter in ECs. Hjv was
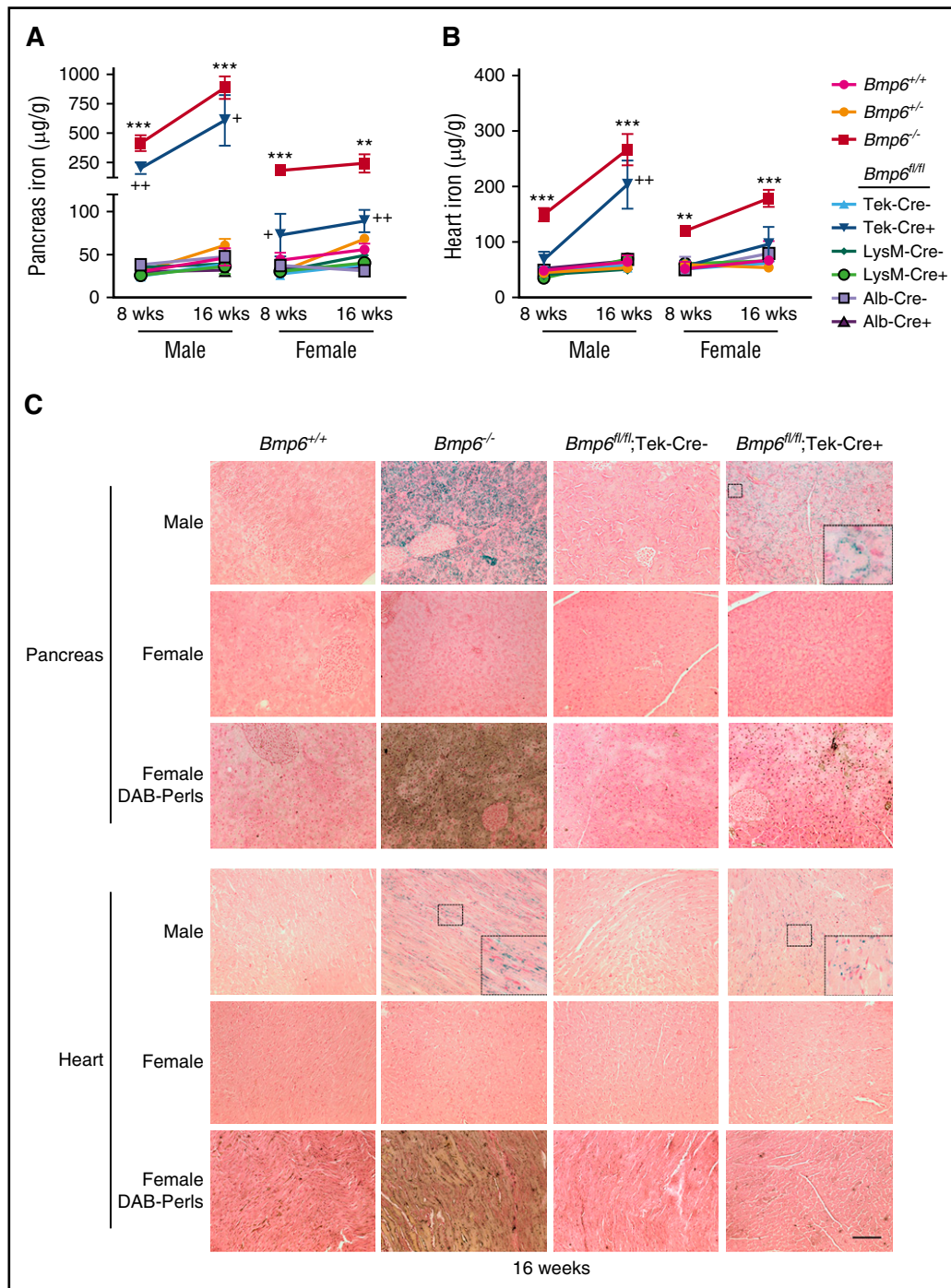
Figure 5. _Bmp6_^{fl/fl};Tek-Cre+ mice exhibit extrahepatic iron loading, whereas _Bmp6_^{fl/fl};Alb-Cre+ and _Bmp6_^{fl/fl};LysM-Cre+ mice do not. Eight- and 16-week-old littermate male and female _Bmp6_^{+/+}, _Bmp6_^{+/−}, and _Bmp6_^{−/−} global knockout mice and _Bmp6_ conditional knockout mice in ECs (_Bmp6_^{fl/fl};Tek-Cre+), macrophages (_Bmp6_^{fl/fl}; LysM-Cre+), and hepatocytes (_Bmp6_^{fl/fl};Alb-Cre+) compared with littermate controls (_Bmp6_^{fl/fl};Cre−) from Figure 4 were analyzed for tissue iron in (A,C) pancreas and (B,C) heart by (A-B) biochemical analysis or (C) Perls' Prussian blue. Diaminobenzidine (DAB)-enhanced Perls' stain was performed on sections that appeared negative or faint by standard Perls' Prussian blue. n = 4 to 7 mice per group (supplemental Table 2), with tissues from 1 representative mouse shown in (C) (original magnification ×20; scale bar represents 100 μM; boxed areas shown enlarged ×5 for pancreas and ×3 for heart in insets for some panels). **_P_ < .01, ***_P_ < .001 relative to control _Bmp6_^{+/+} mice by one-way ANOVA with Dunnett's post hoc test; +_P_ < .05, ++_P_ < .01 relative to control _Bmp6_^{fl/fl};Cre− mice by Student _t_ test.

predominantly expressed on the sinusoidal membrane of hepatocytes immediately adjacent to SEC membranes (Figure 6). Thus, Hjv is poised to respond to locally produced Bmp6 secreted by liver SECs to regulate hepcidin expression in hepatocytes. No significant changes were detected in Hjv protein expression or localization in _Bmp6_^{−/−} compared with _Bmp6_^{+/+} mice (supplemental Figure 9).

Discussion

Inability to appropriately regulate hepcidin production in response to iron loading or deficiency contributes to the pathogenesis of several iron homeostasis disorders. Regulation of liver _BMP6_ mRNA expression is
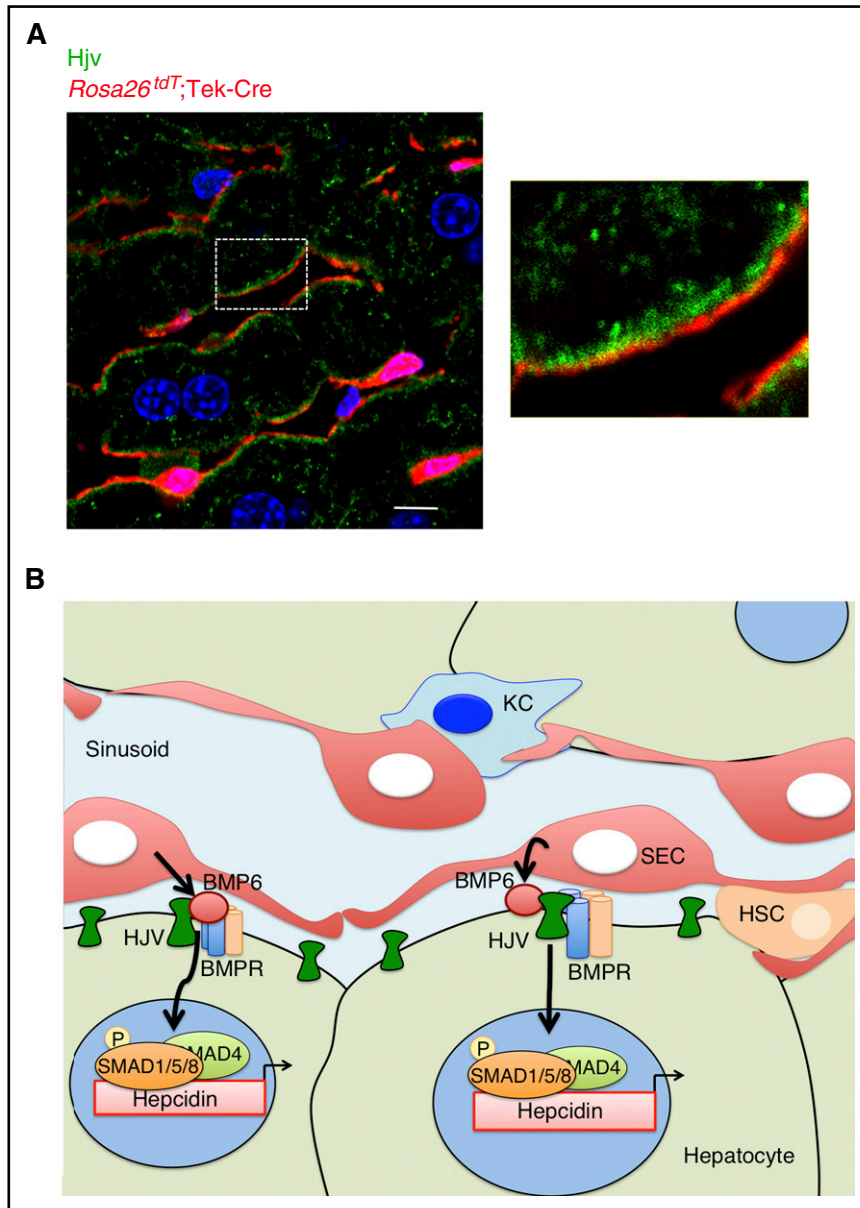
Figure 6. Hjv is expressed in hepatocyte sinusoidal membranes adjacent to Bmp6-producing SECs. (A) Immunofluorescence microscopy of liver tissue from *Rosa26*^tdT;Tek-Cre+ mice. Liver SECs are labeled with tdT (red). Hjv expression is visualized with anti-Hjv antibody (green). Nuclei are labeled with DAPI (blue). Scale bar represents 10 μM. Right panel shows boxed area enlarged ×3. (B) Proposed model: BMP6 is produced in liver SECs and acts in a paracrine fashion on hepatocytes to bind the co-receptor HJV, which together with BMP type I and type II receptors induces SMAD1/5/8 phosphorylation and hepcidin transcription.

a key mechanism by which iron levels control hepcidin expression. Here, we used mice with a conditional ablation of *Bmp6* in different liver cell populations to demonstrate that ECs are the predominant source of Bmp6 critical for hepcidin and iron homeostasis regulation, whereas KCs and hepatocytes do not have a major functional role.

A central role of ECs in Bmp6 production for iron homeostasis regulation is supported by the findings of hepcidin deficiency and iron overload in *Bmp6*^fl/fl;Tek-Cre+ mice. A complicating factor is that the Tek-Cre is not fully specific for ECs. Indeed, the Tek-Cre was previously reported to cause germline recombination, particularly in females,[34] and to be expressed in some hematopoietic cells, including macrophages.[36] Although recent data have recognized the yolk sac rather than the bone marrow origin of KCs and many other resident tissue macrophages under homeostatic conditions, yolk sac progenitors also transiently express the Tek receptor tyrosine kinase.[33] We therefore carefully evaluated the specificity of the Tek-Cre in our models using Cre reporter mice and *Bmp6* genomic DNA and RNA expression

analysis. Germline recombination was detected in 30% to 100% of offspring from female Tek-Cre mice; however, no germline recombination was seen in offspring from Tek-Cre male mice, which were therefore used for subsequent analysis. Interestingly, tdT expression and *Bmp6* recombination was seen not only in ECs but also in KCs from *Rosa26*^tdT;Tek-Cre+ and *Bmp6*^fl/fl;Tek-Cre+ mice. The activity of Tek-Cre in KCs and most likely other resident tissue macrophages should therefore be taken into account in future studies using this Cre strain. Importantly, the lack of iron phenotype in *Bmp6*^fl/fl;LysM-Cre+ mice, in which Cre-mediated recombination also occurs in KCs and other myeloid cells,[30,32] effectively rules out a major role for these cell types in Bmp6 production for hepcidin regulation. A major role for hepatocytes is also excluded by the absence of iron overload in *Bmp6*^fl/fl;Alb-Cre+ mice.

Our data not only exclude a major functional role for KCs and hepatocytes in Bmp6 production for iron homeostasis regulation, but also suggest that hepatocytes and KCs do not produce Bmp6. This provides an important clarification to the literature in which gradient

ultracentrifugation and magnetic-activated cell sorting have been used to isolate ~95% pure liver cell populations, wherein *Bmp6* mRNA levels were only ~3- to 20-fold higher in ECs compared with KCs,[22-24] and *Bmp6* mRNA seemed to be upregulated by iron in most liver cell types.[23,24] Moreover, iron-inducible Bmp6 protein expression was previously reported in hepatocytes by immunohistochemistry.[19,25] In this study, we achieved a greater purity (≥99%) of KCs and ECs using a FACS-based method, which demonstrated ~30- to 80-fold higher *Bmp6* mRNA levels in isolated ECs than in KCs. Unexpectedly, *Bmp6* mRNA levels were not further reduced in isolated KCs of *Bmp6*^fl/fl^; LysM-Cre+ mice or in hepatocytes of *Bmp6*^fl/fl^;Alb-Cre+ mice, even in the context of iron loading. This was not the result of inefficient Cre-mediated recombination because abundant tdT fluorescence was seen in the expected cell type in Cre-reporter mice. Moreover, loss of the floxed *Bmp6* allele and the presence of recombined *Bmp6* allele were clearly detected in the expected cell type by PCR of genomic DNA. Importantly, the relative expression level of *Bmp6* in isolated ECs compared with KCs and hepatocytes closely mirrored the relative expression level of the EC-specific marker *Cd146* in each cell fraction. Moreover, *Bmp6* mRNA was significantly reduced in all liver cell types of *Bmp6*^fl/fl^;Tek-Cre+ mice despite no evidence of Tek-Cre activity in hepatocytes in Cre-reporter mice or genomic DNA evaluation, in which EC contamination would be less evident because of smaller variations in DNA expression among cell types. Together, these data suggest that hepatocytes and KCs do not express *Bmp6* and that the *Bmp6* detected in isolated KCs and hepatocytes in our study and described in prior publications[22-24] is most likely the result of EC contamination. Because *Bmp6* mRNA is much more abundant in ECs than other liver cell types, even a small contamination (~1%) could have a disproportionate effect. The findings of iron-inducible Bmp6 protein expression in hepatocytes previously reported by immunohistochemistry[19,25] may be a consequence of nonspecific antibody binding (which was reported with the same antibodies in immunoblot assays),[19,21] or these assays may detect secreted Bmp6 protein released from ECs that has bound to Hjv and the Bmp receptor complex in hepatocytes.

A predominant role for ECs, but not hepatocytes or KCs, in liver BMP6 production is consistent with the strong reduction in total liver *Bmp6* mRNA expression in *Bmp6*^fl/fl^;Tek-Cre+, but not *Bmp6*^fl/fl^;Alb-Cre+ or *Bmp6*^fl/fl^;LysM-Cre+ mice. However, *Bmp6*^fl/fl^;Tek-Cre+ mice still had detectable liver *Bmp6* mRNA, whereas *Bmp6*^−/−^ mice did not. This is likely due, at least in part, to incomplete efficiency of Cre-mediated recombination in ECs, since low *Bmp6* levels were still detectable in isolated ECs of *Bmp6*^fl/fl^;Tek-Cre+ mice. Another liver cell type, possibly HSCs, could also have a minor contributory role in Bmp6 production. This residual liver *Bmp6* expression in *Bmp6*^fl/fl^; Tek-Cre+ mice, but not *Bmp6*^−/−^ mice, most likely explains the phenotype differences between mice. Although they exhibited similar degrees of serum and liver iron overload, *Bmp6*^fl/fl^;Tek-Cre+ mice tended to have higher *Hamp* mRNA, particularly in males, and reduced extrahepatic iron loading compared with sex-matched *Bmp6*^−/−^ mice. In extrahepatic tissues, heart was loaded later and to a lesser degree than pancreas. A similar but more pronounced pattern of increased *Hamp* mRNA and less extrahepatic iron loading was also seen in female compared with male *Bmp6*^−/−^ and *Bmp6*^fl/fl^;Tek-Cre+ mice. This sex-related dimorphism is consistent with that in a prior study in *Bmp6*^−/−^ mice attributed to the *Hamp*-suppressive effects of testosterone.[35] The authors postulated that lower hepcidin levels in male *Bmp6*^−/−^ mice allowed a greater or faster accumulation of nontransferrin-bound iron available for uptake by extrahepatic tissues.[35] Differential kinetics of iron uptake in liver and extrahepatic tissues, with a threshold behavior for extrahepatic loading with respect to liver iron concentration and earlier loading

in pancreas compared with heart, has been well described in thalassemia patients.[37-39]

The data from the *Bmp6*^fl/fl^;Tek-Cre mice do not exclude a role for Bmp6 production from extrahepatic ECs in hepcidin regulation. However, *Bmp6* mRNA seems to be regulated by iron exclusively in the liver.[18-21] Indeed, *Bmp6* expression in spleen[18] and heart is not induced by a high iron diet. The ability of iron to upregulate intestinal Bmp6 expression reported in 1 study[40] was not corroborated in numerous other studies,[18-21] and the specificity of the Bmp6 antibody in the original study[40] has been questioned.[19,21] Moreover, circulating Bmp6 levels are extremely low.[21] Thus, Bmp6 is most likely functioning locally in the liver to regulate hepcidin.

Our data suggest a model in which liver SECs produce BMP6, which has paracrine actions on the co-receptor HJV in hepatocytes to regulate hepcidin production (Figure 6B). Although HJV binds BMP6 with high affinity and is well-established to augment BMP6 induction of hepcidin expression,[14,41,42] HJV is not required for BMP6 signaling or hepcidin regulation.[42-44] Indeed, BMP6 still induces hepcidin in *Hjv*^−/−^ primary hepatocytes, albeit to a lesser degree than in wild-type hepatocytes.[42] Moreover, hepcidin is still inducible by iron to some extent in *Hjv*^−/−^ mice.[43] This raises the possibility that BMP6 could regulate hepcidin independent of HJV, at least when HJV is unavailable; however, there is no evidence that BMP6 regulates hepcidin independent of HJV under normal conditions.

In summary, our findings reveal a crucial role for ECs in the production of BMP6 for hepcidin and iron homeostasis regulation. Another liver cell population, possibly HSCs, may also have a minor role. However, our data exclude a major role for hepatocytes and KCs in BMP6 production and expose the limitations of liver cell isolation protocols. These findings are a critical step toward understanding the complex regulatory network by which iron levels are sensed by the liver to regulate hepcidin production and how this process goes awry in iron homeostasis disorders.

Acknowledgments

Authorship

Contribution: S.C. performed experiments, interpreted data, and wrote the paper; K.B.Z.-B. initiated the generation of the *Bmp6* floxed, global, and conditional knockout mice; A.B.C. helped with mouse studies and performed immunofluorescence microscopy; C.-Y.W. helped with mouse studies; R.B. helped with immunofluorescence microscopy; M.N. and F.K.S. assisted with fluorescence-activated cell

sorting experiments, and J.L.B. conceived and oversaw the study, interpreted data, and wrote the paper.

Conflict-of-interest disclosure: J.L.B. has ownership interest in Ferrumax Pharmaceuticals, which has licensed technology from the Massachusetts General Hospital on the basis of work cited here and in prior publications. The remaining authors declare no competing financial interests.

Correspondence: Jodie L. Babitt, Massachusetts General Hospital, 185 Cambridge St, CPZN-8208, Boston, MA 02114; e-mail: babitt.jodie@mgh.harvard.edu.

References

1. Ganz T. Systemic iron homeostasis. *Physiol Rev*. 2013;93(4):1721-1741.

2. Nemeth E, Tuttle MS, Powelson J, et al. Hepcidin regulates cellular iron efflux by binding to ferroportin and inducing its internalization. *Science*. 2004;306(5704):2090-2093.

3. Pietrangelo A. Genetics, Genetic Testing, and Management of Hemochromatosis: 15 Years Since Hepcidin. *Gastroenterology*. 2015;149(5): 1240-1251.e4.

4. Roetto A, Papanikolaou G, Politou M, et al. Mutant antimicrobial peptide hepcidin is associated with severe juvenile hemochromatosis. *Nat Genet*. 2003;33(1):21-22.

5. Papanikolaou G, Samuels ME, Ludwig EH, et al. Mutations in HFE2 cause iron overload in chromosome 1q-linked juvenile hemochromatosis. *Nat Genet*. 2004;36(1):77-82.

6. Huang FW, Pinkus JL, Pinkus GS, Fleming MD, Andrews NC. A mouse model of juvenile hemochromatosis. *J Clin Invest*. 2005;115(8): 2187-2191.

7. Niederkofler V, Salie R, Arber S. Hemojuvelin is essential for dietary iron sensing, and its mutation leads to severe iron overload. *J Clin Invest*. 2005; 115(8):2180-2186.

8. Lesbordes-Brion JC, Viatte L, Bennoun M, et al. Targeted disruption of the hepcidin 1 gene results in severe hemochromatosis. *Blood*. 2006;108(4): 1402-1405.

9. Gkouvatsos K, Wagner J, Papanikolaou G, Sebastiani G, Pantopoulos K. Conditional disruption of mouse HFE2 gene: maintenance of systemic iron homeostasis requires hepatic but not skeletal muscle hemojuvelin. *Hepatology*. 2011;54(5):1800-1807.

10. Chen W, Huang FW, de Renshaw TB, Andrews NC. Skeletal muscle hemojuvelin is dispensable for systemic iron homeostasis. *Blood*. 2011; 117(23):6319-6325.

11. Zumerle S, Mathieu JR, Delga S, et al. Targeted disruption of hepcidin in the liver recapitulates the hemochromatotic phenotype. *Blood*. 2014; 123(23):3646-3650.

12. Babitt JL, Huang FW, Wrighting DM, et al. Bone morphogenetic protein signaling by hemojuvelin regulates hepcidin expression. *Nat Genet*. 2006; 38(5):531-539.

13. Casanovas G, Mleczko-Sanecka K, Altamura S, Hentze MW, Muckenthaler MU. Bone morphogenetic protein (BMP)-responsive elements located in the proximal and distal hepcidin promoter are critical for its response to HJV/BMP/SMAD. *J Mol Med (Berl)*. 2009;87(5): 471-480.

14. Andriopoulos B Jr, Corradini E, Xia Y, et al. BMP6 is a key endogenous regulator of hepcidin expression and iron metabolism. *Nat Genet*. 2009;41(4):482-487.

15. Meynard D, Kautz L, Darnaud V, Canonne-Hergaux F, Coppin H, Roth MP. Lack of the bone morphogenetic protein BMP6 induces massive iron overload. *Nat Genet*. 2009;41(4):478-481.

16. Daher R, Kannengiesser C, Houamel D, et al. Heterozygous Mutations in BMP6 Pro-peptide Lead to Inappropriate Hepcidin Synthesis and Moderate Iron Overload in Humans. *Gastroenterology*. 2016;150(3):672-683.e4.

17. Kautz L, Meynard D, Monnier A, et al. Iron regulates phosphorylation of Smad1/5/8 and gene expression of Bmp6, Smad7, Id1, and Atoh8 in the mouse liver. *Blood*. 2008;112(4):1503-1509.

18. Corradini E, Meynard D, Wu Q, et al. Serum and liver iron differently regulate the bone morphogenetic protein 6 (BMP6)-SMAD signaling pathway in mice. *Hepatology*. 2011;54(1): 273-284.

19. Kautz L, Besson-Fournier C, Meynard D, Latour C, Roth MP, Coppin H. Iron overload induces BMP6 expression in the liver but not in the duodenum. *Haematologica*. 2011;96(2):199-203.

20. Zhang AS, Gao J, Koeberl DD, Enns CA. The role of hepatocyte hemojuvelin in the regulation of bone morphogenic protein-6 and hepcidin expression in vivo. *J Biol Chem*. 2010;285(22): 16416-16423.

21. Pauk M, Grgurevic L, Brkljacic J, et al. Exogenous BMP7 corrects plasma iron overload and bone loss in Bmp6-/- mice. *Int Orthop*. 2015;39(1): 161-172.

22. Feng Q, Migas MC, Waheed A, Britton RS, Fleming RE. Ferritin upregulates hepatic expression of bone morphogenetic protein 6 and hepcidin in mice. *Am J Physiol Gastrointest Liver Physiol*. 2012;302(12):G1397-G1404.

23. Enns CA, Ahmed R, Wang J, et al. Increased iron loading induces Bmp6 expression in the non-parenchymal cells of the liver independent of the BMP-signaling pathway. *PLoS One*. 2013;8(4): e60534.

24. Rausa M, Pagani A, Nai A, et al. Bmp6 expression in murine liver non parenchymal cells: a mechanism to control their high iron exporter activity and protect hepatocytes from iron overload? *PLoS One*. 2015;10(4):e0122696.

25. Kautz L, Meynard D, Besson-Fournier C, et al. BMP/Smad signaling is not enhanced in Hfe-deficient mice despite increased Bmp6 expression. *Blood*. 2009;114(12):2515-2520.

26. Zumbrennen-Bullough KB, Wu Q, Core AB, et al. MicroRNA-130a is up-regulated in mouse liver by iron deficiency and targets the bone morphogenetic protein (BMP) receptor ALK2 to attenuate BMP signaling and hepcidin transcription. *J Biol Chem*. 2014;289(34):23796-23808.

27. Jenkitkasemwong S, Wang CY, Coffey R, et al. SLC39A14 Is Required for the Development of Hepatocellular Iron Overload in Murine Models of Hereditary Hemochromatosis. *Cell Metab*. 2015;22(1):138-150.

28. Kisanuki YY, Hammer RE, Miyazaki J, Williams SC, Richardson JA, Yanagisawa M. Tie2-Cre transgenic mice: a new model for endothelial cell-lineage analysis in vivo. *Dev Biol*. 2001;230(2): 230-242.

29. Bagnall AJ, Kelland NF, Gulliver-Sloan F, et al. Deletion of endothelial cell endothelin B receptors does not affect blood pressure or sensitivity to salt. *Hypertension*. 2006;48(2):286-293.

30. Vujić Spasić M, Kiss J, Herrmann T, et al. Hfe acts in hepatocytes to prevent hemochromatosis. *Cell Metab*. 2008;7(2):173-178.

31. Postic C, Magnuson MA. DNA excision in liver by an albumin-Cre transgene occurs progressively with age. *Genesis*. 2000;26(2):149-150.

32. Clausen BE, Burkhardt C, Reith W, Renkawitz R, Förster I. Conditional gene targeting in macrophages and granulocytes using LysMcre mice. *Transgenic Res*. 1999;8(4):265-277.

33. Gomez Perdiguero E, Klapproth K, Schulz C, et al. Tissue-resident macrophages originate from yolk-sac-derived erythro-myeloid progenitors. *Nature*. 2015;518(7540):547-551.

34. Koni PA, Joshi SK, Temann UA, Olson D, Burkly L, Flavell RA. Conditional vascular cell adhesion molecule 1 deletion in mice: impaired lymphocyte migration to bone marrow. *J Exp Med*. 2001; 193(6):741-754.

35. Latour C, Kautz L, Besson-Fournier C, et al. Testosterone perturbs systemic iron balance through activation of epidermal growth factor receptor signaling in the liver and repression of hepcidin. *Hepatology*. 2014;59(2):683-694.

36. Constien R, Forde A, Liliensiek B, et al. Characterization of a novel EGFP reporter mouse to monitor Cre recombination as demonstrated by a Tie2 Cre mouse line. *Genesis*. 2001;30(1): 36-44.

37. Wood JC. Guidelines for quantifying iron overload. *Hematology (Am Soc Hematol Educ Program)*. 2014;2014(1):210-215.

38. Meloni A, Restaino G, Missere M, et al. Pancreatic iron overload by T2* MRI in a large cohort of well treated thalassemia major patients: can it tell us heart iron distribution and function? *Am J Hematol*. 2015;90(9):E189-E190.

39. Noetzli LJ, Papudesi J, Coates TD, Wood JC. Pancreatic iron loading predicts cardiac iron loading in thalassemia major. *Blood*. 2009; 114(19):4021-4026.

40. Arndt S, Maegdefrau U, Dorn C, Schardt K, Hellerbrand C, Bosserhoff AK. Iron-induced expression of bone morphogenic protein 6 in intestinal cells is the main regulator of hepatic hepcidin expression in vivo. *Gastroenterology*. 2010;138(1):372-382.

41. Wu Q, Sun CC, Lin HY, Babitt JL. Repulsive guidance molecule (RGM) family proteins exhibit differential binding kinetics for bone morphogenetic proteins (BMPs). *PLoS One*. 2012;7(9):e46307.

42. Canali S, Core AB, Zumbrennen-Bullough KB, et al. Activin B Induces Noncanonical SMAD1/5/8 Signaling via BMP Type I Receptors in Hepatocytes: Evidence for a Role in Hepcidin Induction by Inflammation in Male Mice. *Endocrinology*. 2016;157(3):1146-1162.

43. Ramos E, Kautz L, Rodriguez R, et al. Evidence for distinct pathways of hepcidin regulation by acute and chronic iron loading in mice. *Hepatology*. 2011;53(4):1333-1341.

44. Latour C, Besson-Fournier C, Meynard D, et al. Differing impact of the deletion of hemochromatosis-associated molecules HFE and transferrin receptor-2 on the iron phenotype of mice lacking bone morphogenetic protein 6 or hemojuvelin. *Hepatology*. 2016;63(1):126-137.